Superalloys 2012: 12th International Symposium on Superalloys
Edited by: Eric S. Huron, Roger C. Reed, Mark C. Hardy, Michael J. Mills, Rick E. Montero, Pedro D. Portella, Jack Telesman
TMS (The Minerals, Metals & Materials Society), 2012

A Proposal on Quantitative Treatment of Multiple Cracks Nucleating in Single Crystal Superalloys

Yasuhiro MUKAI[1], Hiroyuki KAGAWA[1]
[1]The Kansai Electric Power Co., Inc.; 3-11-20, Nakoji, Amagasaki, Hyogo, 661-0974, Japan

Keywords: Single crystal, Superalloy, Multiple crack propagation behavior, Crack propagation rate

Abstract

Multiple crack propagation tests were performed at room temperature using four point bending specimens which contained nineteen cracks and were made of Ni-based single crystal superalloy CMSX-4. Two types of specimen orientations were machined. One's longitudinal direction was [010] and machined notch direction was [100], and another's was [010] and [101]. In each specimen, cracks propagated along {111} slip planes making ridges which inclined to the thickness direction. The cracks of the former also inclined to the longitudinal direction at an angle of 45°, while those of the latter propagated along the machined notch direction. To evaluate such crack propagation behavior, mode I - III stress intensity factors were calculated under three conditions. First, cracks were treated as single edge crack without considering crack interaction. Secondly, cracks were treated as multiple parallel edge cracks with same lengths. Third, cracks were treated as multiple parallel edge cracks with alternately different lengths. Since stage-I cracking was evaluated by resolved shear stress intensity factor range on {111} plane, resolved shear stress intensity factor was calculated from mode I - III stress intensity factors obtained by the above three conditions. Then, crack propagation simulations were performed. In case of the [010][101] orientation specimen, simulated crack propagation rates and behavior calculated under the third condition agreed well with the experimental ones. On the other hand, in case of the [010][100] specimen, those calculated by the first condition agreed better with the experiments than those simulated by the other conditions.

Introduction

Cracking is often produced in blades and nozzles of a gas turbine power plant by thermal stress [1, 2]. One of the authors previously inspected the discarded blades which had been used for 20,000 hour (200 cycles of operation) in a 1300°C class gas turbine power plant, and found the existence of multiple parallel cracks at outer surface of the leading edge. Those cracks were perpendicular to the axial direction and penetrated from the corrosion-resistant coating layer to the substrate [3]. The initiation mechanism of these cracks is regarded as the following. When a gas turbine shuts down, tensile stress is created in a coating layer on outer-surfaces of blades. Since at relatively low temperature the coating is brittle [4], cracks are generated from the coating layer and propagate through the substrate. Because components of gas turbines are expensive, the method for evaluating the crack propagation behavior is needed to draw up an adequate repair criterion and to lower maintenance costs of these components.

One of the authors previously estimated the thermal and centrifugal stress of first stage blades, and created the equations for calculating stress intensity factor (SIF) of multiple parallel edge (MPE) cracks which were placed on a semi-infinite plate and subjected to arbitrarily distributed stress [3]. With the estimated stress and SIF equations, crack propagation simulations for MPE cracks on blade surface were carried out. As the result, the simulated crack length was roughly consistent with observed depth on blade surface if the crack interval of MPE cracks was suitably selected in the evaluations. In the above case, the simulated and observed crack length on blade surface was 1mm. After the cracks grow longer with subsequent start-ups and shut-downs, some cracks may propagate selectively longer than the other cracks. To confirm that, additional studies were carried out with MPE crack propagation tests using four-point-bending specimens [5]. The result was that almost all cracks grew at similar growth rates at first, then some cracks propagated rapidly while cracks on either side of them propagated slowly. To simulate such crack propagation behavior, we proposed the equation for estimating SIFs of MPE cracks whose lengths were alternately different. With this equation, crack propagation simulations were performed. As the result, the simulated crack length distribution agreed well with experimental ones.

1500°C class gas turbine power plants use single crystal or directionally solidified Ni-based superalloys for first stage blades. In such superalloys, crystallographic cracking may occur and propagate on {111} slip planes [6, 7]. If MPE cracks propagate on {111} slip plane with inclined angle, the neighboring cracks can possibly cross each other, and the blade may partially break. In this study, single crystal superalloy CMSX-4 was used for a fundamental research of crystallographic MPE cracking. Two types of orientation specimens were made. MPE crack propagation tests were carried out at room temperature in four-point-bending load. The effect of crystallographic cracking on MPE crack propagation behavior was examined. The applicability of the above equations [3, 5] for polycrystalline materials to single crystal material was also studied.

Experimental Procedure

The material used in this study is Ni-based single crystal superalloy CMSX-4. The mass% chemistry of the material was 6.4%Cr, 9.5%Co, 3.0%Re, 6.3%W, 0.6%Mo, 6.5%Ta, 1.0%Ti, 5.4%Al, 0.10%Hf, and balance Ni. The cast plates were solution treated at 1586K for 2 hours, 1573K for 10 hours, 1586K for 2 hours, 1589K for 2 hours, 1591K for 2 hours and 1594K for 2 hours, and aged at 1353K for 4 hours and 1144K for 20 hours. Two kinds of orientation specimens were made: TP-A and TP-B. In TP-A, the longitudinal direction is [010] and the machined notch direction is [100]; in TP-B, the former is [010] and the latter is [101]. The geometry of the specimens is shown in Figure 1a. The thickness is 10mm.

Pre-cracks were introduced by eccentric tension-compression load under 1Hz at room temperature. Since a crack was initiated at a curved portion in the opposite side of the machined notch during pre-cracking, specimens were machine again into the shape as shown in Figure 1b to eliminate the crack.

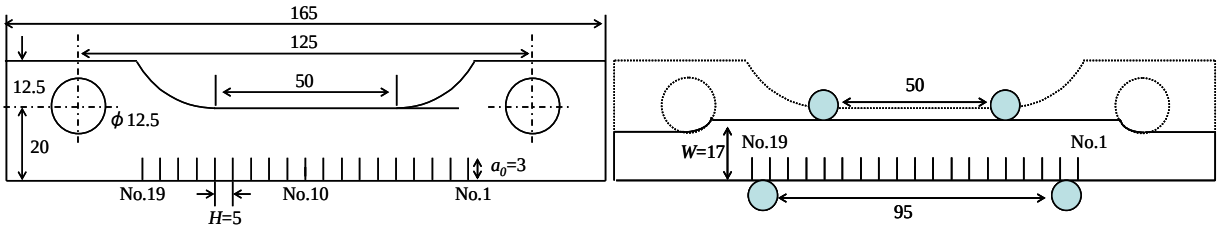

(a) Eccentric tension-compression specimen (b) Four-point-bending specimen

Figure 1. Geometries of specimens (thickness: 10mm)

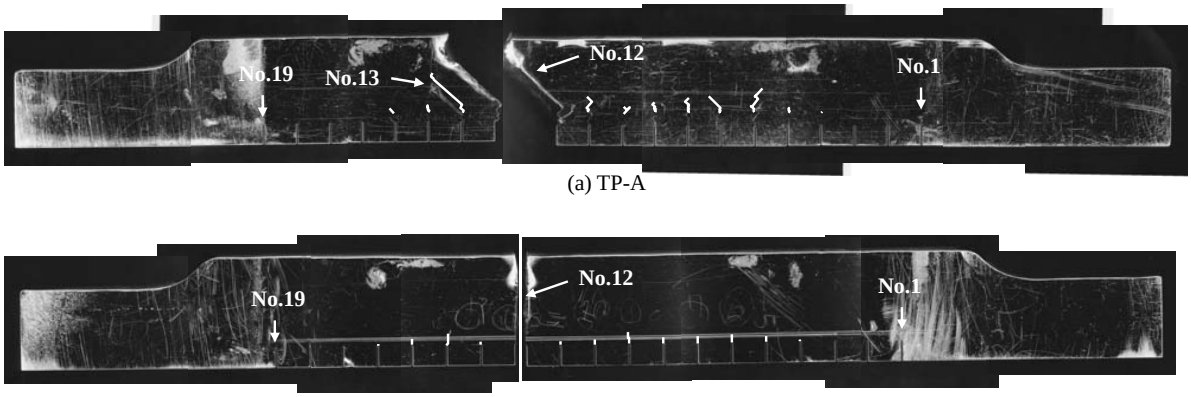

(a) TP-A

(b) TP-B

Figure 2. Appearance of fractured specimens.

The width, *W*, was changed to *W*=17mm. Fatigue crack propagation tests were then performed using the four-point-bending geometry. The inner span was 50mm and the outer span was 95mm. No.5-No.15 cracks (crack No.1 is rightmost and No.19 is leftmost in Figure 1) were placed on the inside of the inner span. Crack lengths were measured by microscope.

Results

Crack propagation behavior

Figure 2 shows a side face in each specimen which was divided forcibly at No.12 crack. In Figure 2, each crack path was emphasized by a white line. In TP-A, cracks propagated at an angle of 45° to the machined notch direction. In TP-B, each cracks propagated along the machined notch direction. Figure 3 shows the fracture surfaces of No.12 crack in each specimen. In TP-A, fracture surfaces consisted of {111} slip planes. In TP-B, though the fracture surface initially consisted of $(\bar{1}11)$ and $(11\bar{1})$ slip planes, it changed to flat after crack length became longer than 5mm. A similar change was observed in the other tests [8] conducted by the authors with compact-type specimens. In case of fcc material whose crack plane is (010) and crack propagation direction is [101], crack propagate possibly by alternating slip [9] at the crack tip because the slip plane was placed symmetrically above and below the crack plane. In the following discussion, it assumed that the ridge-type fracture was continued to the end in TP-B. Figure 4 shows side view of No.13 crack in TP-A. The crack was observed to propagate on a 45° direction macroscopically, but to ±45° with zigzag pattern microscopically. It was also observed that cracks propagated along slip lines shearing the γ' precipitates.

Figure 5 shows the crack length distributions. The abscissa shows crack number and the ordinate shows crack lengths at both side faces of the specimens. Plots and lines represent crack lengths observed on the side shown in Figure 2 and the opposite side, respectively. Since cracks in the TP-A were inclined to the machined notch direction, projected crack length *a*' was employed to the vertical axis in Figure 5a. Projected crack length *a*' is described as $a'=a\cdot\cos\theta$ where θ is an angle between a machined notch direction and a crack propagation direction observed at specimen side face. Crack lengths observed at each side face in TP-B were similar to each other, but those in TP-A were different up to 1mm. The average crack length of both sides was used in the following chapters.

Crack propagation rate

SIFs calculation on condition of single crack. When a stress distribution in a finite width plate without crack is approximated by equation (1), stress intensity factor K_I for single edge crack placed on this plate is calculated by equation (2) [10].

$$\sigma(x/W)=\sum_{i=0}^{n}\sigma_i\cdot(x/W)^i \tag{1}$$

$$K_I=\left\{\sum_{i=0}^{n}f_i(\xi)\cdot\sigma_i\cdot\xi^i\right\}\sqrt{\pi a'} \tag{2}$$

ξ is calculated by $\xi = a'/W$, *x* is distance from the plate edge. $f_i(\xi)$ is a influence factor for single edge crack and is expressed by equation (3).

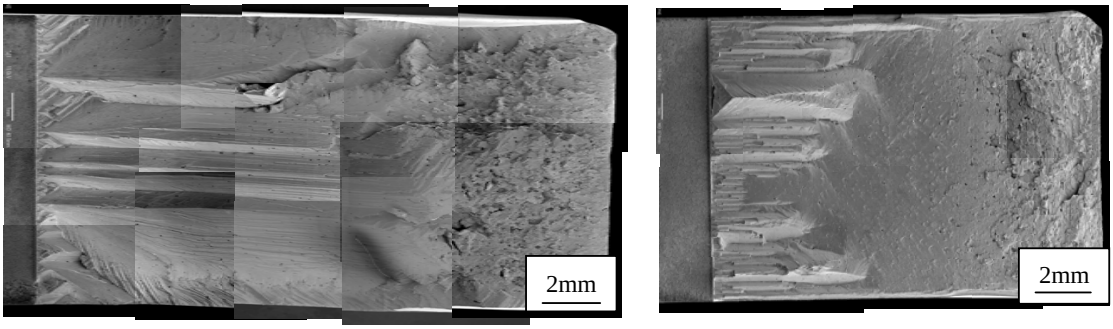

(a) TP-A (Crack No.12) (b) TP-B (Crack No.12)

Figure 3. Fracture surfaces of longest cracks.

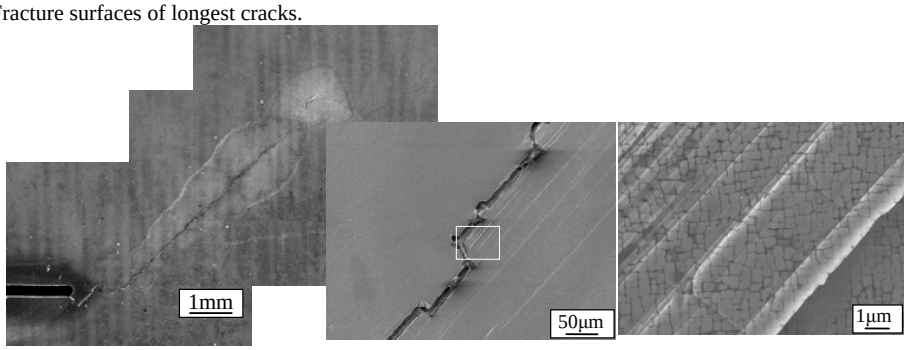

Figure 4. Side viewing of No.13 crack in TP-A. Crack propagated at an angle of 45°, and slip lines along the crack were observed.

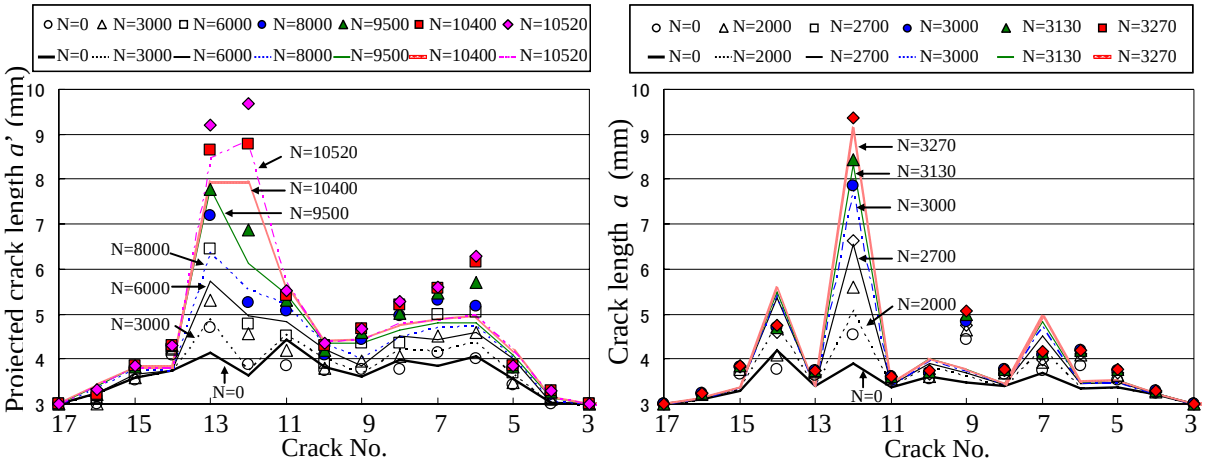

(a) TP-A (b) TP-B

Figure 5. Experimental results of multiple crack propagation tests. The abscissa shows crack number, and the ordinate shows projected crack lengths for TP-A and crack lengths for TP-B in each cycle N. Plots and lines represent crack lengths observed on the side shown in Figure 2 and the opposite side, respectively.

$$f_i(\xi) = \sum_{j=0}^{4} C_{ij} (\xi)^{2j} \qquad (3)$$

The coefficients C_{ij} in equation (3) are described in the reference [10]. Two coordinate systems are considered. First, x-axis is in the machined notch direction, y-axis is in the specimen longitudinal direction and z-axis is in the specimen thickness direction. Secondly, x'-axis is in the crack propagated direction, y'-axis is in the crack plane normal. ϕ is an angle between y'-axis and a normal of a plane on which x'-axis and z-axis lie. In this study, cracks are inclined at angles of θ to the notch normal direction and ϕ to the thickness direction in each specimen. First, the effect of crack inclination at an angle of θ on SIFs was estimated by equation (4) [11].

$$K'_{\mathrm{I}} = B^{\mathrm{I}}(\theta)\cdot(a'/a)^{0.5}\cdot K_{\mathrm{I}}$$
$$K'_{\mathrm{II}} = B^{\mathrm{II}}(\theta)\cdot(a'/a)^{0.5}\cdot K_{\mathrm{I}} \qquad (4)$$

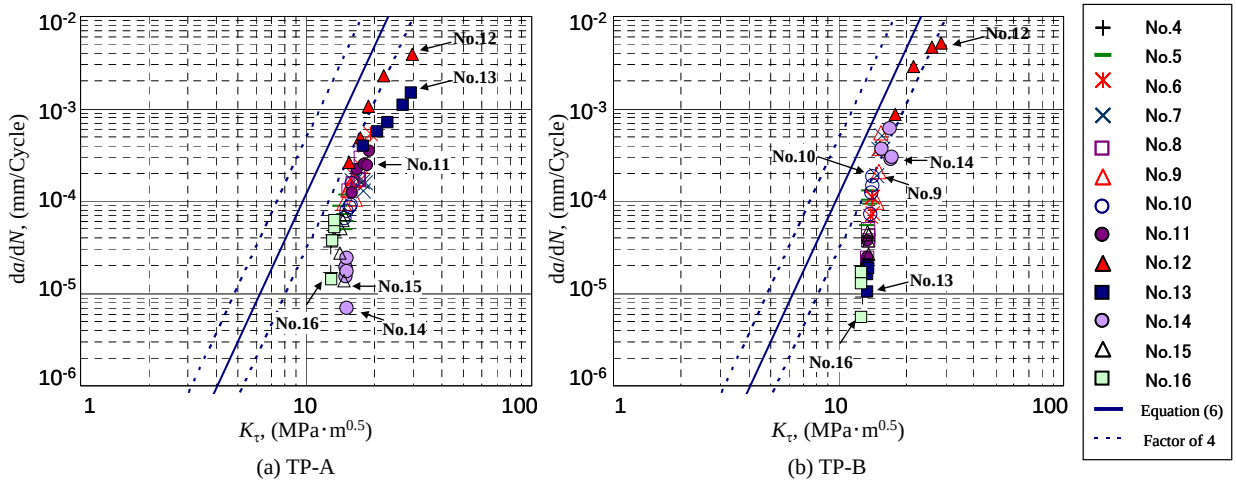

(a) TP-A (b) TP-B

Figure 6. Crack propagation rate da/dN as a function of resolved shear stress intensity factor K_τ. K_τ was calculated on condition that each crack was treated as an independent single crack.

K_I is the value when θ is 0°, which is calculated by equation (2) and (3). K'_I and K'_{II} are the values of a crack inclined at an angle of θ. When θ is 45°, B^I is 0.7049 and B^{II} is 0.3645. Note that equation (4) represents SIFs of single edge crack on a semi-infinite plate. Secondly, the effect of crack inclination at an angle of ϕ was taken into account by equation (5) [12].

$$K''_I = K'_I \cdot \cos^2\phi$$
$$K''_{II} = K'_{II} \cdot \cos^2\phi \qquad (5)$$
$$K''_{III} = K'_I \cdot \cos\phi \cdot \sin\phi$$

K'_I and K'_{II} are the values when ϕ is 0° which are calculated by equation (4). K''_I, K''_{II} and K''_{III} are the values of a crack inclined at an angle of ϕ. Note that ξ was assumed that ξ = a'/W in TP-A.

The authors [8] separately studied the crack propagation rate of CMSX-4 by using compact-type specimens at temperature range between room temperature and 900°C. As the result, the stage-I crack propagation rates were evaluated by equation (6) to be in the range of a factor of 4.

$$da/dN = 8.69 \cdot 10^{-10} \cdot K_\tau^{5.11} \qquad (6)$$

K_τ [13] is a resolved stress intensity factor range, which is calculated by equation (7).

$$K_\tau = \lim_{r \to 0} \sqrt{2\pi r (\sigma_{x'y'}^2 + \sigma_{y'z'}^2)} = \sqrt{K''^2_{II} + K''^2_{III}} \qquad (7)$$

r is distance from crack tip.

Figure 6 shows the crack propagation rates of multiple crack propagation tests as a function of K_τ which were calculated by equations (2)-(5) and (7). The crack propagation rates were calculated by five-point-incremental-polynomial approach. The solid line represents equation (6) and the dot-lines show the range of factor of 4. FCF data for both specimens was plotted below the solid line. The slopes of da/dN –ΔK_τ plots of No.12 and No.13 in TP-A were comparable to that of the line. On the other hand, in TP-B almost all plots except No.12 crack were arrayed vertically near ΔK_τ=15. Since MPE crack propagation rates were not evaluated successfully by the above equations, other approaches were considered in the following section.

Discussion

SIFs calculations and crack propagation rate estimations

SIFs of inclined single edge cracks. In the previous section, the effect of crack inclination at an angle of θ on SIFs was approximately estimated by equation (4). Since such estimation was thought to be a source of error, FEA was performed to calculate SIFs of θ =45° inclined crack. SIFs of single edge crack inclined at an angle of θ =45° were expressed by equation (8) and (9).

$$K'_P = \left\{ \sum_{i=0}^{1} f'^P_i(\xi) \cdot \sigma_i \cdot \xi^i \right\} \sqrt{\pi a'} \qquad (P = \text{I, II}) \qquad (8)$$

$$f'^P_i(\xi) = \sum_{j=0}^{4} C_{ij}^P \cdot (\xi)^j \qquad (i=0,1\ ,\ P = \text{I, II}) \qquad (9)$$

ξ is ξ =a'/W. f^I_i and f^{II}_i are influence factors of single inclined edge crack. To calculate the influence factors, single edge crack propagating from the machined notch at an angle of θ =45° was modeled in the range from a'=3.5mm to 10mm. Figure 7 shows the model for example. For evaluating bending load, i was confined to i = 0 and 1. Stress distribution, σ_0=1 and $\sigma_1 = 1 \cdot (x/W)$, were applied at crack faces, and then the influence factors, f^I_i and f^{II}_i were calculated by stress extrapolation method. FEM calculation was performed by MSC-Marc 2010 [14] under plane strain with four-node-quadrilateral-elements. Number of elements was about 100,000. The node distance between crack tip nodes along crack plane was 0.005mm. The influence factors calculated by FEA were formulated in the form of equation (9). The coefficient C_{ij}^P is listed in Table I. Then, K_τ was obtained from equation (5), (7), (8) and (9). Figure 8 shows crack propagation rates of TP-A as a function of K_τ. A lot of plots in Figure 8 were placed around the lower bound of factor of 4.

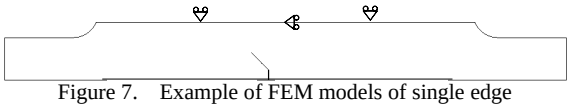

Figure 7. Example of FEM models of single edge crack in TP-A.

Table I. Coefficients of Equation 9 for single edge crack in TP-A.

	TP-A (Single crack)			
	F_0^{I}	F_0^{II}	F_1^{I}	F_1^{II}
C_{i0}^{n}	0.948	0.127	0.522	-0.048
C_{i1}^{n}	-2.272	2.181	-1.354	3.036
C_{i2}^{n}	18.208	-5.724	9.108	-10.348
C_{i3}^{n}	-35.832	9.475	-17.264	16.941
C_{i4}^{n}	36.849	-2.305	15.888	-8.983

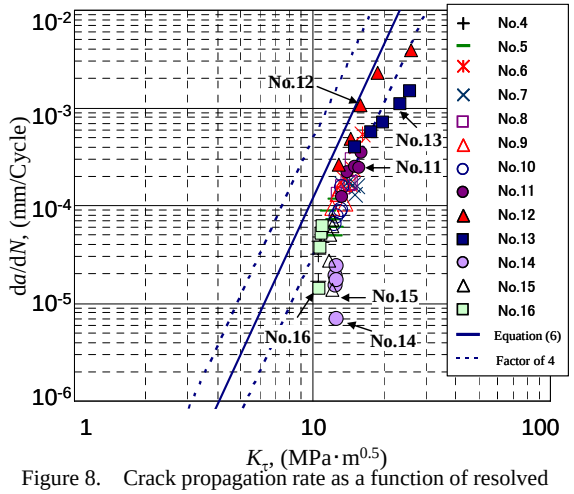

Figure 8. Crack propagation rate as a function of resolved shear stress intensity factor K_τ. K_τ was calculated on condition that each crack was treated as single crack.

SIFs for MPE cracks with same lengths. Influence factors of MPE cracks with same lengths were calculated by FEM. MPE cracks with same lengths placed in four-point-bending specimens were modeled. The relations between influence factors and SIFs are shown in equation (10).

$$K'_P = \left\{ \sum_{i=0}^{1} F_i^P(\xi) \cdot \sigma_i \cdot \xi^i \right\} \sqrt{\pi a'} \quad (P\text{=I, II}) \tag{10}$$

$$F_i^P(\xi) = \sum_{j=0}^{4} C_{ij}^{\ P} \cdot (\xi)^j \quad (i\text{=0, 1 , } P\text{=I, II}) \tag{11}$$

F_i^{I} is influence factor for mode I SIF and F_i^{II} is for mode II SIF. FEM model for TP-A is shown in Figure 9. For the TP-B, MPE cracks propagating in the machined notches direction were modeled in the range from a=3mm to 10mm. Stress distributions, σ_0=1, σ_1 = 1·(x/W), were applied at crack faces. And then, the influence factors, F_0^{I}, F_1^{I} were calculated by stress extrapolation method. For TP-A, MPE cracks propagating from the machined notches at an angle of θ =45° were modeled in the range from a'=3.5mm to 10mm. The influence factors, F_0^{I}, F_1^{I}, F_0^{II} and F_1^{II} were calculated. The influence factors calculated by FEM were formulated in the form of equation (10). The coefficients $C_{ij}^{\ P}$ are listed in Table II. Note that, in the TP-B, ξ is substituted to ξ= a'/W.

Figure 10 shows crack propagation rates as a function of K_τ which was calculated by equations (5), (7), (10) and (11). In case of TP-A, contrary to Figure 8 where most of plots were located around the lower bound of factor of 4, most of plots in Figure 10a were located in the upper half of factor of 4. In case of TP-B, contrary to Figure 6b, most of plots located within the range of factor of 4. However, in TP-B, the plots except for No.12 crack were still arrayed vertically. This method was inadaptable to evaluate crack propagation rate at lower K_τ in TP-B, because SIFs of short length cracks adjacent to long cracks were lower than those calculated by equation (10) and (11).

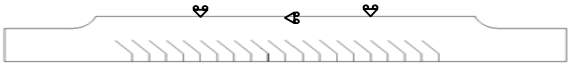

Figure 9. Example of FEM models of multiple parallel cracks with same length in TP-A.

Table II. Coefficients of Equations 11 for multiple parallel edge crack with same lengths in TP-A and TP-B.

	TP-B		TP-A			
	F_0^{I}	F_1^{I}	F_0^{I}	F_0^{II}	F_1^{I}	F_1^{II}
C_{i0}^{n}	1.000	0.483	0.705	-0.052	0.231	0.012
C_{i1}^{n}	-4.797	-0.968	-2.951	3.479	0.661	2.338
C_{i2}^{n}	29.165	7.708	19.009	-12.482	0.815	-9.966
C_{i3}^{n}	-57.972	-16.083	-39.005	21.343	-4.634	18.245
C_{i4}^{n}	54.861	16.890	38.292	-8.841	8.466	-10.169

SIFs of MPE cracks with alternately different length. SIFs of MPE cracks with alternately different lengths are expressed by equations (12).

$$K'_P = \left\{ F_0^{\ P} \cdot h_0^{\ P} \cdot \sigma_0 + F_1^{\ P} \cdot h_1^{\ P} \cdot \xi \cdot \sigma_1 \right\} \sqrt{\pi a'} \quad (P\text{=I, II}) \tag{12}$$

$h_{\mathrm{i}}^{\mathrm{I}}$ and $h_{\mathrm{i}}^{\mathrm{II}}$ are influence factors. $h_{\mathrm{i}}^{\mathrm{I}}$ describes the difference of the mode I SIF between MPE cracks with same lengths and those with alternately different lengths, and $h_{\mathrm{i}}^{\mathrm{II}}$ does that for mode II SIF. Since the detail of the influence factor $h_{\mathrm{i}}^{\mathrm{I}}$ was described in the reference [5], the outline is shown here. When cracks with length a and cracks with length a^* are distributed alternately, $h_{\mathrm{i}}^{\mathrm{I}}$ of cracks with length a is calculated by equation (13) - (16).

$$h_i^{\mathrm{I}} = \frac{b_i \exp(C_i \varsigma)}{\exp(C_i \varsigma) + (b_i - 1)\exp(-C_i \varsigma)} \tag{13}$$

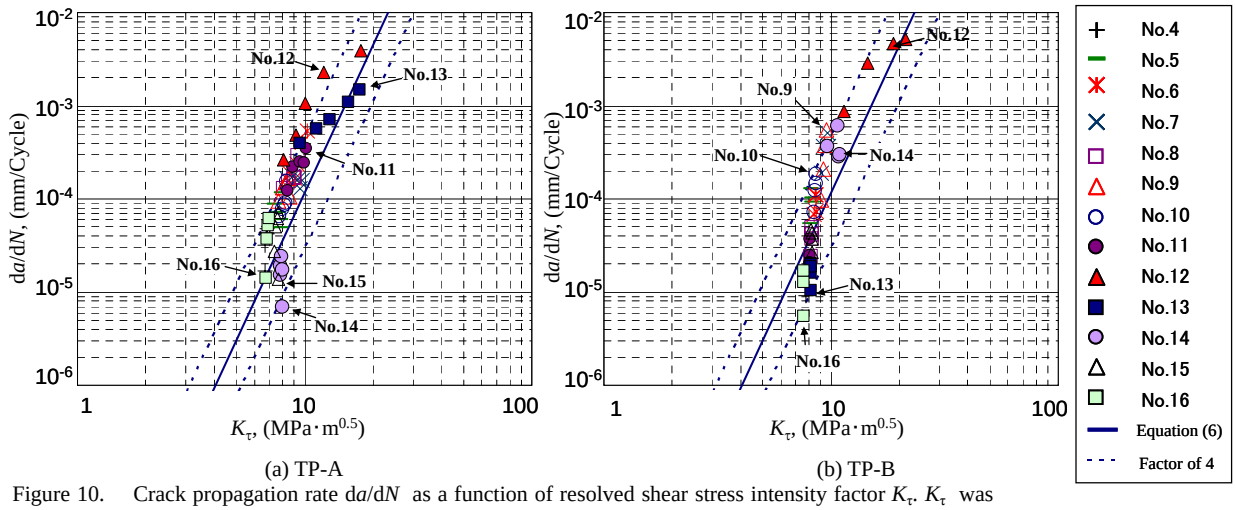

(a) TP-A (b) TP-B

Figure 10. Crack propagation rate da/dN as a function of resolved shear stress intensity factor K_τ. K_τ was calculated on condition that individual cracks were treated as multiple parallel cracks with same length.

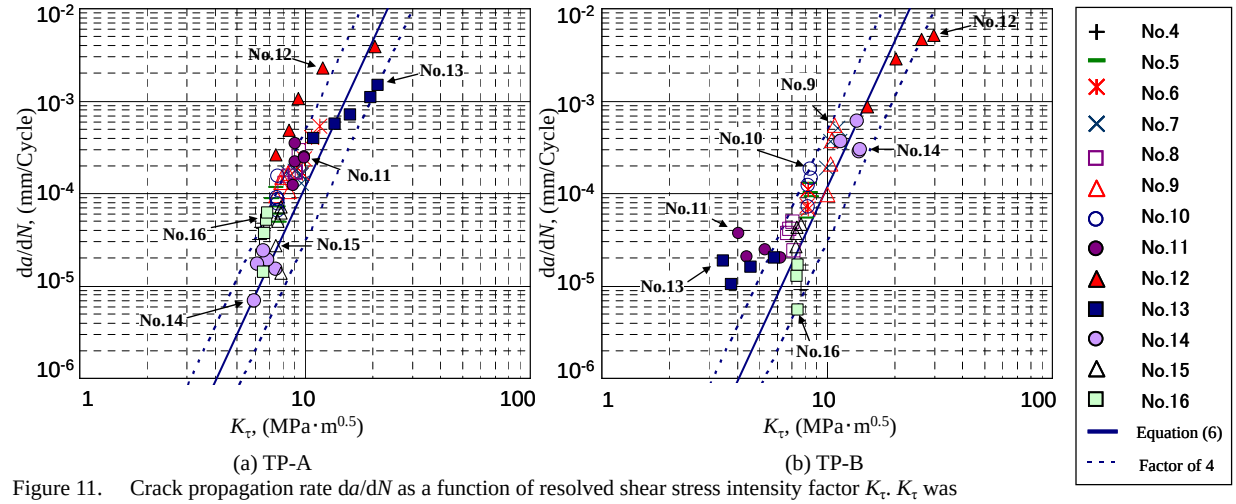

(a) TP-A (b) TP-B

Figure 11. Crack propagation rate da/dN as a function of resolved shear stress intensity factor K_τ. K_τ was calculated on condition that multiple parallel but different length cracks were distributed alternately.

$$b_i = \frac{g_i(\xi,2\eta)}{g_i(\xi,\eta)} \tag{14}$$

$$C_0 = 1.080(\xi/\eta)^3 - 2.925(\xi/\eta)^2 + 5.341\xi/\eta \tag{15}$$

$$C_1 = 2.250(\xi/\eta)^3 - 7.352(\xi/\eta)^2 + 9.705\xi/\eta \tag{16}$$

ζ is $\zeta = \ln(a/a^*)$, η is $\eta = H/W$. $g_i(\xi,\eta)$ and $g_i(\xi,2\eta)$ are the influence factors of MPE cracks where MPE cracks are arrayed infinitely with interval of H and $2H$, respectively. These values are shown in the reference [3]. h_i^I becomes 1 when a/a^* becomes 1, and becomes 0 when a/a^* becomes 0. When a/a^* becomes larger, the effect of cracks with length a^* becomes smaller. Therefore, SIF of alternately different lengths comes close to SIF of cracks with crack interval $2H$; h_i^I comes close to b_i. For calculating the h_i^I of No.j crack with crack length a_j, it was assumed that cracks whose lengths were a_j and $a^*=(a_{j+1}+a_{j-1})/2$ were distributed alternately. In case of TP-B, h_i^I was calculated from equations (13)-(16), and then K_τ was evaluated with equations (5), (7), (11) and (12). In case of TP-A, though h_i^I calculated by equations (13)-(16) was used for estimating mode I SIF, h_i^{II} is unknown. To estimate the h_i^{II}, several FEM calculations were performed, in which alternately different length cracks were modeled using four-point-bending specimen geometry. As the result, the effect of alternate distribution of crack lengths on mode II SIF was not remarkable, compared to that on mode II SIF. Therefore, h_i^{II} is approximately assumed as $h_i^{II}=1$ for all range of ζ. Then, K_τ for TP-A was calculated by equations (5), (7) and (11)-(16) with the assumption of $h_i^{II}=1$.

Figure 11 shows crack propagation rates as a function of K_τ obtained from the above process. While the lower K_τ plots of TP-B were placed vertically around K_τ=8-9MPa·m$^{0.5}$ in Figure 10b, these plots in Figure 11b were located along the solid-line. Crack propagation rates in TP-B were evaluated within the range of factor of 4, except for No.11 and No.13 data. On the other hand, in TP-A, the difference of plots distribution between Figure 10a and Figure 11a is small. That was because of the assumption of $h_i^{II}=1$.

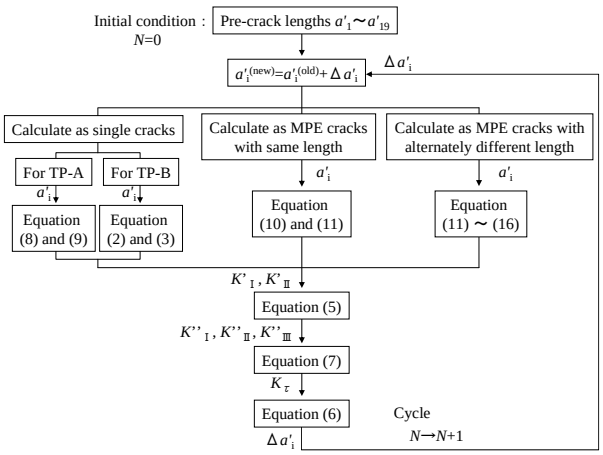

Figure 12. Flow chart for crack propagation simulation.

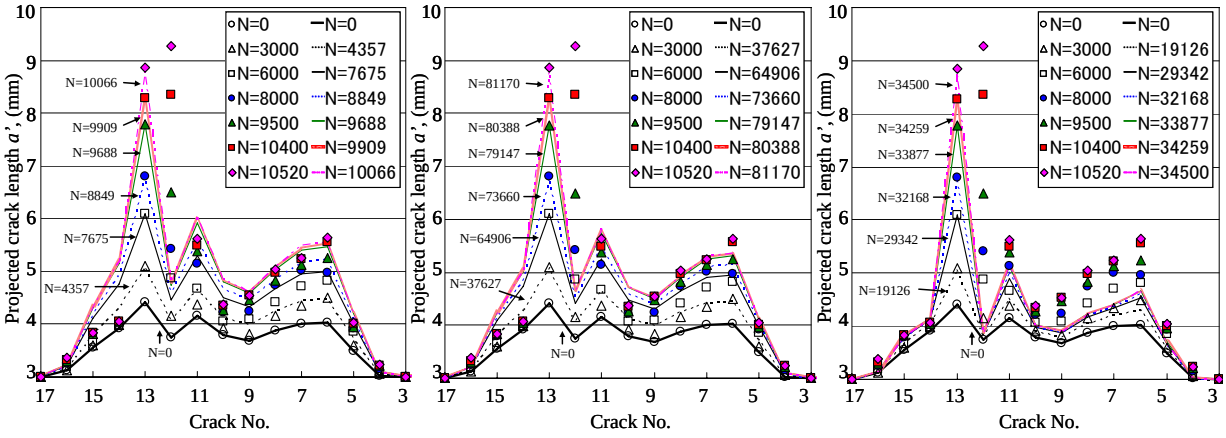

(a) Simulated as single crack. (b) Simulated as multiple same length crack (c) Simulated as multiple different length crack distributed alternately

Figure 13. Relation between experimental and simulated crack distributions of TP-A. Plots indicate experimental crack length and lines indicate simulated crack length.

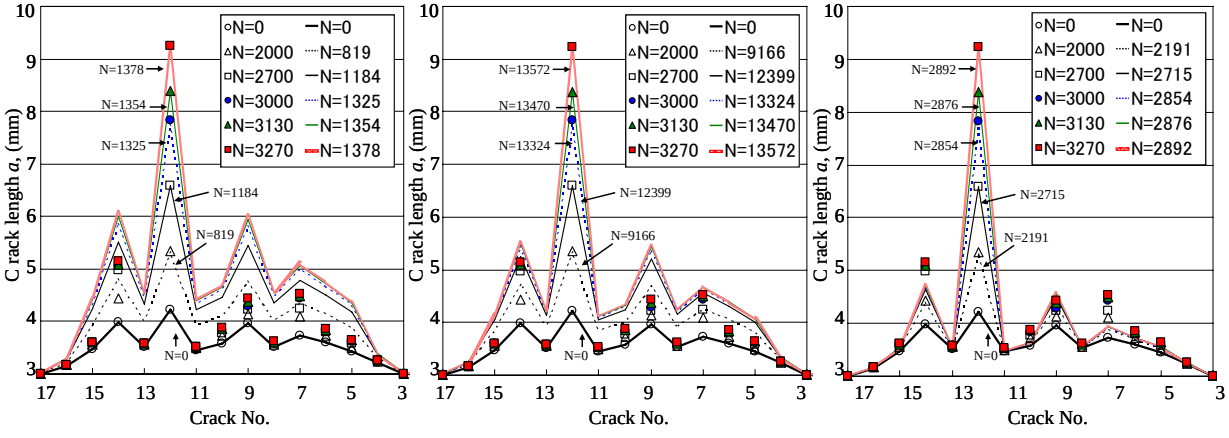

(a) Simulated as single crack. (b) Simulated as multiple same length crack (c) Simulated as multiple different length crack distributed alternately

Figure 14 Relation between experimental and simulated crack distributions of TP-B. Plots indicate experimental crack length and lines indicate simulated crack length.

Crack propagation simulation

Crack propagation simulations were performed for the three methods used to treat the effect of crack interaction. In the first method, crack interaction was not considered and each crack was treated as single crack represented by equation (2) for TP-B and equation (8) for TP-A. In the second method, crack interaction was treated as MPE cracks with same lengths represented by equation (10). In the third method, crack interaction was treated as MPE cracks with alternately different lengths represented by equation (12). Figure 12 shows the flow chart of the simulations. Pre-crack distributions were considered as initial conditions of simulations (N=0). K_τ was calculated from crack length distribution by each method, and crack propagation increment Δa_i was calculated by equation (6).

Figure 13 and 14 show the simulation results of TP-A and TP-B, respectively. In each figure, the experimental crack lengths are shown as solid symbols with the experimental cycle N, and the simulated crack lengths are shown as solid lines with simulated cycle N when the simulated crack length of crack No.13 for TP-A and No.12 for TP-B reached experimental ones. In TP-B, the simulated crack length distribution and number of cycle calculated by considering the influence of alternately different crack lengths agreed with experimental ones. On the other hand, in TP-A, simulated results calculated on condition that each crack acts as single crack were closer to experimental ones. In TP-A, crack length of No.13 was longest among all cracks before N=9500, but it was passed by No.12 crack when N reached N=10400. Since all simulated methods stated above could not explain such behavior, simulated crack length of No.12 in TP-A never agreed with experimental one.

One of the reasons is that in case of inclined cracks the influence factor h_i^{II} of shorter crack could be larger than that of longer crack. To confirm that, another FEM calculation was performed, in which only two cracks emanating from machined notches in four-point-bending specimen were modeled as follows. The modeled crack length of No.12 and No.13 crack were a'=8.5mm and a'=9mm, respectively. Note that in the FEM model No.12 crack inclined as if it covered the outer side of No.13 crack. As the result, though K_I of the shorter crack No.12 was smaller than that of the longer crack No.13, K_{II} of crack No.12 was larger than that of crack No.13. That is possibly one of the reasons why No.12 crack passed the No.13 crack which had largest pre-crack length.

Conclusion

Multiple crack propagation behavior of Ni-based superalloy CMSX-4 was examined. Multiple crack propagation tests were performed at room temperature with two specimen orientations. The combinations of the specimen longitudinal direction and machined notch direction were [010][100] (TP-A) and [010][101] (TP-B). The results were as following.

1. In TP-A, each crack propagated at an angle of 45° from the machined notch direction to the specimen longitudinal direction, while in TP-B each crack propagated along the machined notch direction. Each fractured surface consisted of {111} planes with ridges inclined to the specimen thickness direction.
2. Three types of crack propagation simulations were performed to evaluate the multiple crack propagation rates and behavior. First, cracks were treated as a single crack. Secondly, cracks are treated as multiple parallel edge cracks with the same lengths. Third, cracks are treated as multiple parallel edge cracks with alternately different lengths. The result was that crack propagation rates and length distribution in TP-B were well simulated by the third method but those in TP-A were not well simulated by this method. In TP-A, the first method was better than the others in simulating experimental crack length distributions. It was caused by the assumption that mode II stress intensity factor of multiple parallel inclined edge cracks with alternately different lengths was the same as those of the cracks with same lengths.
3. In TP-A, though crack No.13 had longest pre-crack length, crack No.12 passed No.13 during the test. FEM calculation showed that in case of inclined multiple cracks, mode II stress intensity factor of the shorter crack could be larger than that of the longer crack in some cases.

References

1. H.L.Bernstein and J.M.Allen, “Analysis of cracked gas turbine blades“, Journal of Engineering for Gas Turbines and Power, Vol.114(1992), pp.293-301.

2. Russel ES. Practical life prediction methods for thermal-mechanical fatigue of gas turbine buckets. In: Weiss V, Bakker WT, editors. Proceedings of Conference on life prediction for high-temperature gas turbine materials, EPRI Repot AP-4477, 1986. p.(3-1)-(3-39).

3. Morita A. Kagawa H. Kubo S. Evaluation of multiple crack propagation behavior in a gas turbine blade under thermal fatigue condition. In: Rodery CD. Takagi Y, editors. Fitness for service, life extension, remediation, repair and erosion/corrosion issues for pressure vessels and components, ASME/JSME Pressure Vessels and Piping Conference PVP-Vol.471, 2004. pp43-49.

4. Wood MI. The mechanical properties of coatings and coated systems. Mater Sci Engng. 1989; A121: p633-643.

5. H. Kagawa, A. Morita, T. Matsuda and S. Kubo, ”Fatigue crack propagation behavior in four-points bending specimens with multiple parallel edge notches at regular intervals”, Engineering Fracture Mechanics, (2008), vol.75, pp.4594-4609.

6. J.Telesman and L. J. Ghosn, “Fatigue crack growth behavior of PWA 1484 single crystal superalloy at elevated temperatures”, Journal of Engineering for Gas Turbines and Power, Volume 118(1996), 399-405

7. P. A. S. Reed, X. D. Wu and I. Sinclair, “Fatigue crack path prediction in UDIMET 720 nickel-based alloy single crystals”, Metallurgical and Materials Transactions A, Volume 31A(2000), 109-123

8. Y. Mukai, H. Kagawa, “The effect of crystal orientation and temperature on fatigue crack growth of Ni-based single crystal superalloy”, Superalloys 2012, submitted.

9. P. Neumann, “New experiments concerning the slip progresses at propagating fatigue cracks I”, Acta metallurgica, Volume 22(1974), 1155-1165

10. Anderson TL. Thorwald G. Revelle DJ. Osage DA. Janelle JL. Fuhry ME. Development of stress intensity factor solutions for surface and embedded cracks in API579. WRC Bulletin 471, 2002.

11. Murakami Y. Stress intensity factors handbook, Vol.4, pp.150, Elsevier Science Ltd, 2001.

12. K. S. Chan, J. E. Hack and G. R. Leverant, “Fatigue crack propagation in Ni-base superalloy single crystals under multiaxial cyclic loads”, Metallurgical Transactions A, Volume 17A(1986), 1739-1750

13. M.Okazaki, M.Sakaguchi, and S.Yamanobe, "Fatigue crack propagation behavior significantly interacting with microstrucural units in thin wall Ni-base superalloy structures", 10th International Gas Turbine Congress, IGTC11, Osaka, Japan, November.13-18,2011.

14. MSC.Marc 2010. Online Manual, 2010, MSC software.